Journal of Applied Physics ARTICLE scitation.org/journal/jap

A study of strain-induced indirect-direct bandgap transition for silicon nanowire applications

Cite as: J. Appl. Phys. **125**, 082520 (2019); doi: 10.1063/1.5052718
Submitted: 21 August 2018 · Accepted: 17 November 2018·
Published Online: 10 December 2018

Song Li,[1] Jyh-Pin Chou,[1] Hongti Zhang,[1,2] Yang Lu,[1,2,a)] and Alice Hu[1,a)]

AFFILIATIONS

[1]Department of Mechanical Engineering, City University of Hong Kong, Kowloon Tong, Hong Kong, China
[2]Center for Advanced Structural Materials (CASM), Shenzhen Research Institute of City University of Hong Kong, Shenzhen, China

[a)]Authors to whom correspondence should be addressed: yanglu@cityu.edu.hk and alicehu@cityu.edu.hk

ABSTRACT

Recently, ultralarge (>10%) strain with fully reversible elastic deformation has been experimentally achieved in silicon nanowires [H. Zhang *et al.*, Sci. Adv. **2**, e1501382 (2016)]. With this breakthrough, here in this work, based on the first principles calculation, the structural and electric properties of silicon under ultralarge strain are comparatively investigated. Unlike previous theoretical/simulation investigations on silicon nanowires with only a few nanometers, bulk silicon models are employed here to provide more realistic and comparable results to our experimentally tested samples (~100 nm diameter). Strong anisotropic effects are induced by loading strain along all different orientations. Simultaneously, the band structures evolution demonstrates electronic anisotropy with the loading strain on three orientations. Silicon keeps an indirect bandgap under increased strain along the ⟨100⟩ orientation while transforming to a direct bandgap with strain along ⟨110⟩ and ⟨111⟩ orientations. Furthermore, ultralarge strain on these two orientations would diminish the bandgap and result into metallization. These results provide insights into understanding "elastic strain engineering" of silicon nanowire applications and demonstrate the possibility of tuning the electronic and optical properties through pure mechanical straining of functional materials.

INTRODUCTION

Strain engineering is a powerful strategy that is employed to achieve significant optimization in functional materials and device performance.[1–9] Among plenty of research studies, strain engineering on group-IV materials is drawing the most attention owing to its vast applications in mechanics, electronics, and photonics. Silicon is of vital importance owing to the role of silicon nowadays in the semiconductor industry,[10,11] covering from high-speed integrated circuits to building blocks in the microelectromechanical system (MEMS) and nanoelectromechanical system (NEMS). High elasticity silicon is needed to satisfy the requirement of mechatronics applications in field effect transistors,[12] biosensing,[13] and high speed detectors.[14] Therefore, further investigations are imperative to achieve large elastic strain.

Previous reports demonstrate that the materials would become much stronger mechanically when the size of the materials is down to nanoscale such as thin films, nanowires, and nanoparticles.[4,15–17] This may be attributed to their high surface-to-volume ratio, defect-scarce status, and smooth surface.[6] This opens a possible way to realize large elastic strain and thus further tune the physical and chemical properties. Based on this, recently, we successfully realized ultralarge and fully reversible elastic deformation on silicon nanowires (~100 nm).[6,18] The tensile strain reached 16%; much closer to the theoretical prediction of 20%.[19–21] Naturally, these works motivate us to investigate the structural and electronic properties of silicon under ultralarge strain. Many research studies have been performed during the past few decades to study the strain related structural and electronic property evolution both theoretically and experimentally,[20–30] but few investigations demonstrated whether ultralarge strain would bring different and novel phenomena.

The advantage of computational simulation is its ability to provide reliable and efficient ways to systematically study the electronic structure of nanomaterials. Plenty of theoretical works have been performed to investigate the structural and electronic properties of silicon nanowires. Rurali investigated

bare surface silicon nanowires and obtained conducting characteristics owing to the energetically favorable surface reconstructions.[31] Surface modifications could diminish undesirable surface states derived from surface unstable dangling bonds. Different surface modifications can remarkably tune the bandgap and the work function of small diameter nanowires.[26,32–34] However, it is technically challenging to perform simulations on electronic properties with models approaching the real size. Hence, in this paper, we utilized first principles calculations to investigate the structural and electronic properties of bulk silicon under varied strains along different orientations. Our results show the indirect-to-direct bandgap transition of silicon under large strain along certain orientations. With further application of elastic strain, the bandgap would vanish and realize metallization.

METHOD

First principle calculations were performed using the Vienna *ab initio* simulation package (VASP)[35,36] based on the density functional theory (DFT) with the projector augmented wave (PAW) method.[37,38] To describe the exchange-correlation interactions, the Perdew-Burke-Ernzerhof (PBE) functional within the generalized gradient approximation (GGA) correction is used.[39] The energy cutoff for the plane

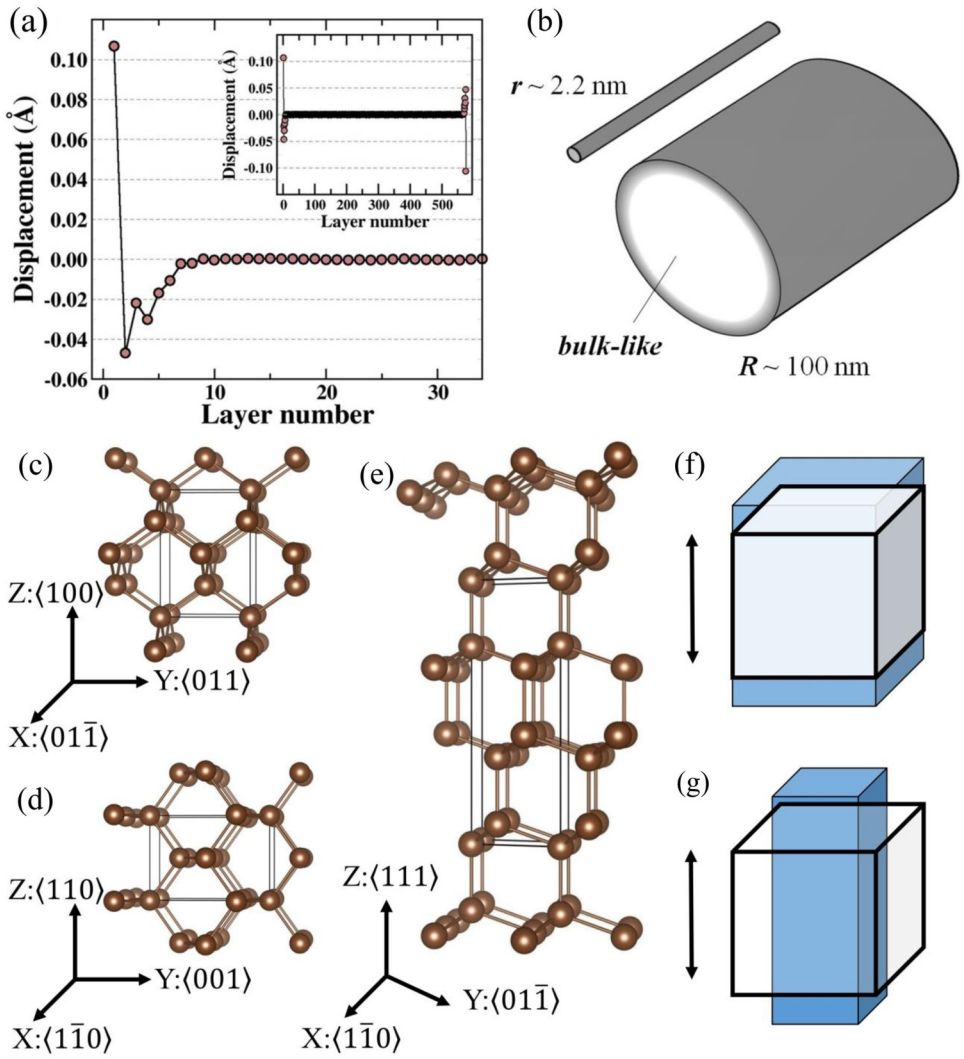

FIG. 1. (a) The interlayer displacement of 35 surface layers of Si (111). The inset panel presents the whole results of the Si (111) surface with 576 layers. (b) The illustration of small and large Si nanowires. The unit cell of bulk silicon of (c) ⟨100⟩, (d) ⟨110⟩, and (e) ⟨111⟩ orientations is shown. The schematic representation of two kinds of loading conditions is shown: (f) unrelaxed tension (without transverse optimization) and (g) relaxed tension (with transverse optimization). The black double-headed arrow represents the direction of loading strain.

wave expansion is set to 250 eV, while Monkhorst-Pack k-points grid are $11\times11\times8$, $11\times8\times11$, and $11\times11\times6$ for ⟨100⟩, ⟨110⟩, and ⟨111⟩ orientations during the geometry optimization. All these calculation parameters were examined as well converged. The threshold for energy is 10^{-5} eV, while for force is 0.01 eV/Å, which can provide reliable accuracy. It is well-known that the PBE functional underestimates the bandgap in most cases,[40] and the PBE bandgap of silicon bulk is 0.71 eV.[41] The Heyd-Scuseria-Ernzerhof (HSE) hybrid functional[42,43] could provide a more reasonable bandgap as 1.11 eV; nevertheless, the calculation is computationally expensive. Thus, we use the Meta-GGA "made simple" (MS1) method,[44,45] which includes the kinetic energy density and, therefore, could provide comparable accuracy with less computational cost than HSE. The calculated MS1 bandgap for bulk silicon is 1.17 eV, which is in good agreement with experimental values.[41]

Heretofore, the pronounced size effects are systematically studied. Results demonstrate that the bandgap decreases to bulk value as the diameters increase owing to the weakened quantum confinement despite the surface modification and orientation of nanowires.[34,46,47] Reports indicate that the quantum size effect can be eliminated, and the indirect bandgap character can be reproduced when the diameter of the silicon nanowire is larger than 7 nm.[26,47] The influence of surface effects and modification gradually decreases on the electronic properties on nanowires.[34] In addition, the study on the silicon thin film also suggests that the surface passivation barely affects the electron states with comparatively large thickness.[48] Therefore, unlike the previous theoretical

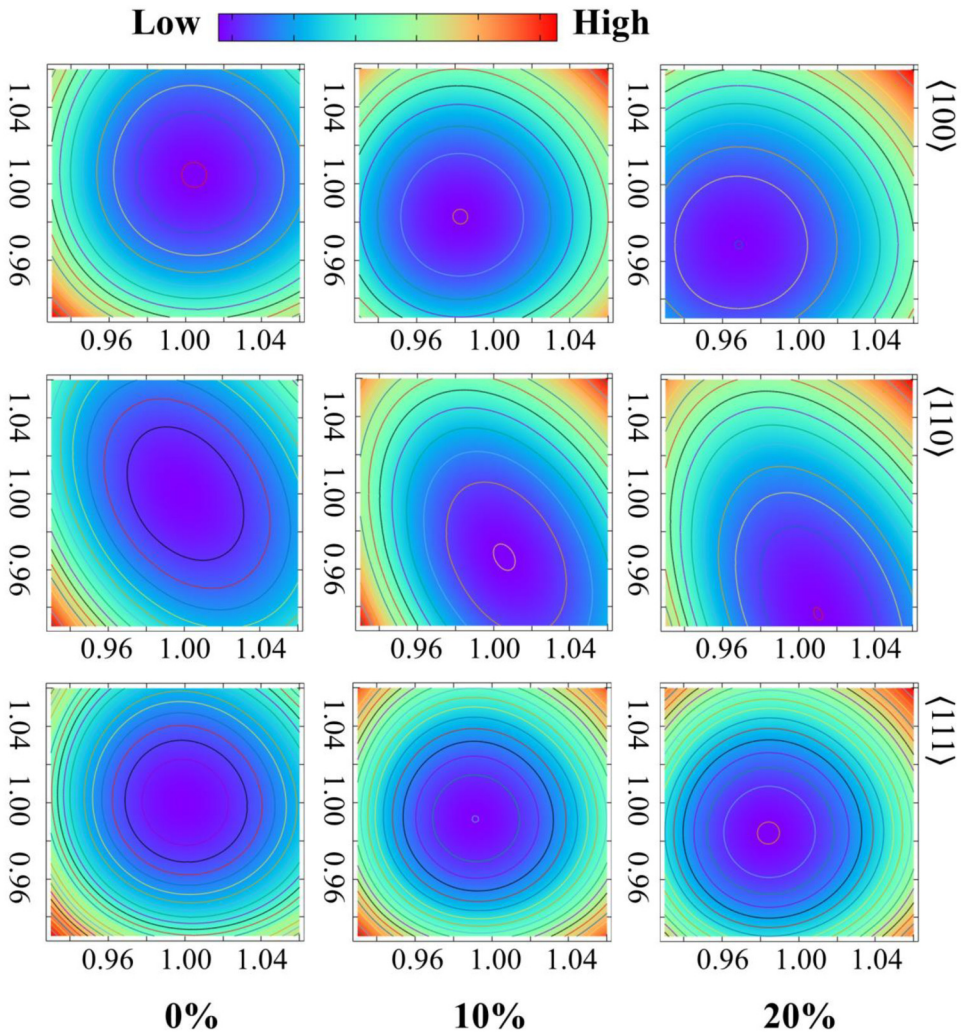

FIG. 2. The PES of the transverse lattice constant of silicon under 0%, 10%, and 20% tensile strain. The x and y axes represent the normalized lattice variation ratio of cross-section geometries with the 0.01 interval. The red and blue colors denote the high and low energies.

work on nanowires,[32,49,50] the periodic bulk silicon model would be a better choice to provide more comparable and realistic simulations of our experimental sample (~100 nm radius).

The optimized lattice constant of silicon is 5.465 Å. To appreciate the size effect on Si, we first calculate the structural variation of Si (111) as an example. We simulate an extremely thick Si (111) surface with a total of 576 Si layers (94.6 nm). The y-axis (displacement) represents the interlayer changes referred to as idea bulk; see Fig. 1(a). As one can see, the displacement rapidly vanishes implying that the surface effect only penetrates a few layers, less than 10 layers; therefore, the electronic properties (e.g., bandgap) for a huge Si nanowire are dominated by "bulk." For the sake of convenience, here, we modeled three kinds of structures to simulate the strain along different crystal orientations or growth directions of the nanowire, which are shown in Fig. 1. The ⟨100⟩, ⟨110⟩, and ⟨111⟩ orientations are considered. The uniaxial strain is applied stepwise on the z directions of all the structures.

RESULTS AND DISCUSSION

To systematically understand the influence of the external strain, two modes of strain loading are calculated here as a comparison.[20] As shown in Figs. 1(f) and 1(g), the unrelaxed tension and the fully relaxed tension are considered here to investigate the cross-section geometry evolution. With the transverse relaxation, the potential energy surfaces (PESs) as a function of the transverse lattice constant under strain silicon are depicted in Fig. 2. The range of the lattice variation ratio is set from 0.93 to 1.06 for each orientation, with an increment of 0.01. The circular PES reveals the isotropic lattice variation for ⟨100⟩ and ⟨111⟩, while the anisotropic behavior of the ⟨110⟩ orientation during the loading strain. Studies have already revealed that Poisson's ratio of ⟨110⟩ does not show a cylindrical symmetry in different orientations.[20,51] In Fig. 3, we summarize the lattice variations with increased strain up to 20%. For the strain applied on silicon ⟨100⟩ orientation, the lattice of X:⟨01$\bar{1}$⟩ and Y:⟨011⟩ uniformly decreases 3% under 20% loading strain. For the strain on ⟨110⟩ orientation, the lattice variation of the Y:⟨001⟩ orientation decreases 6% at 20% strain. Interestingly, the lattice of X:⟨1$\bar{1}$0⟩ increases 1% at 8% external strain. Therefore, the ⟨110⟩ strain would induce the anisotropic Poisson effect. The lattice decrease of X:⟨1$\bar{1}$0⟩ and Y:⟨01$\bar{1}$⟩ is 2% at 20% strain owing to much smaller Young's modulus, which is 169.1 GPa.[52] For the three loading directions, the ⟨111⟩ orientation of silicon shows the least distinct Poisson effect due to the small Poisson's ratio of 0.180,[51] while the ⟨110⟩ orientation shows the distinct Poisson effect owing to a relatively large Poisson's ratio of 0.368.[51] These results reveal that the longitudinal loading strain could induce different transversal deformation in different orientations. In other words, the structural deformation of cross sections is anisotropic for different growth directions of nanowires.

Figure 4 displays the band structures of silicon under strain. For the three different models, the different Brillouin zones and k-paths[53] are selected (see Fig. S1 in the supplementary material). Also, to consider the Poisson effect influence on the band structures, the band structures under unrelaxed and relaxed tension are plotted here. In all the calculations, the positions of valence band maximum are unchanged under external strains. As in the silicon ⟨100⟩ model, the conduct band local minimum valley in the M→Γ interval drops downward, while the local minimum valley in the Γ→Z interval lifts upward. Consequently, the conduct band minimum (CBM) located in the Γ→Z interval shifts leftward to the M→Γ interval with the increasing strain. For a primitive silicon cell, it is known that the CBM lies on the Δ symmetry line near the X point leading to six equivalent valleys Δ_6[27] (see Fig. S2 in the supplementary material). The biaxial tension normal to the axial direction would split the Δ_6 valleys into four higher in-plane valleys Δ_4 and two lower out-plane valleys Δ_2.[54] Correspondingly, the tensile strain in ⟨100⟩ increases the energy of Δ_2 valleys along the direction of strain and decreases the energy of Δ_4 valleys normal to the loading strain direction. Compared to the unrelaxed case, the Poisson effect during relaxed tension would significantly influence the band structure and the Poisson effect becomes stronger as the applied strain increases. The bandgaps are 0.81 eV and 0.46 eV for 10% and 20% unrelaxed tension, while they are 0.61 eV and 0.16 eV for 10% and 20% relaxed tension, respectively. For the ⟨110⟩ orientation model, the original CBM locates in the Y→Γ interval and it shifts rightward to the Γ point as the external strain increases, leading the system to transform from the indirect bandgap to the direct bandgap. Previous theoretical studies reported the indirect to direct bandgap transition on negative strained Si using a linear

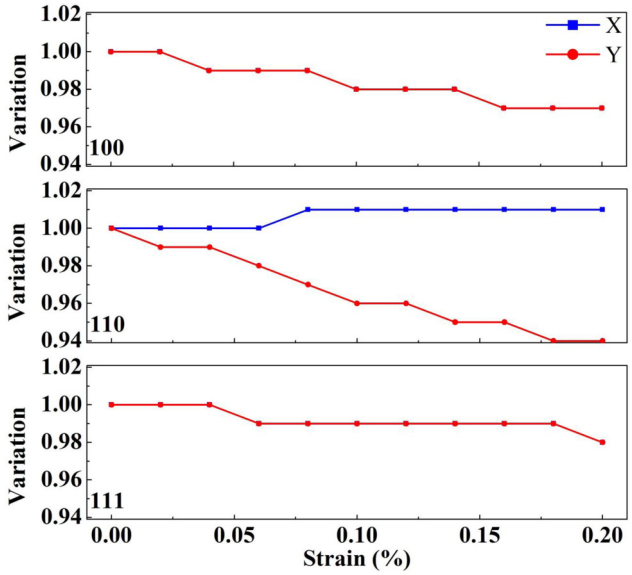

FIG. 3. Lattice variation of silicon under various loading strains from 0% to 20% along ⟨100⟩, ⟨110⟩, and ⟨111⟩ orientations. The blue and red lines indicate the normalized lattice variation along corresponding X and Y directions, respectively.

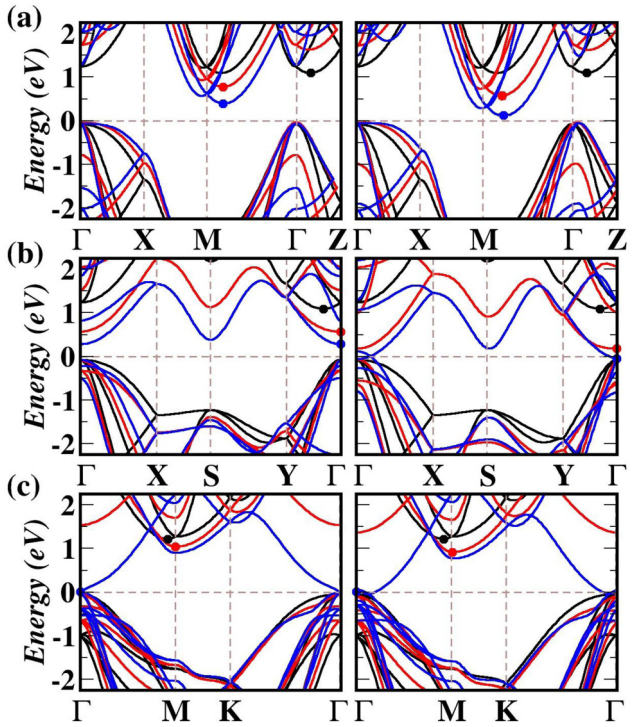

FIG. 4. Band structure of silicon in (a) ⟨100⟩, (b) ⟨110⟩, and (c) ⟨111⟩ structures under various loading strains. Left and right figures are band structures under the unrelaxed tension and relaxed tension conditions. The band structures under 0%, 10%, and 20% strains are denoted by black, blue, and red lines, respectively. The solid circles represent the corresponding CBM positions.

combination of Gaussian orbitals and GW approximation.[55,56] Similarly, compared to the unrelaxed system, the conduction bands in relaxed systems drop more significantly if the Poisson effect is considered. The bandgap of the unrelaxed system is 0.66 eV, while it is 0.24 eV for the relaxed case under 10% strain. More interestingly, the unrelaxed structure still possesses a 0.36 eV bandgap with 20% strain, while the gap would be diminished at the relaxed structure. The Poisson effect would eliminate the direct bandgap of silicon at the Γ point and then induces metallization in 20% ultralarge strain like the previous report.[49] Likewise, the same evolution happened in the silicon ⟨111⟩ bulk structure. The system achieves indirect to direct bandgap transition and metallization under ultralarge strain. The above calculations and analysis indicate that the external strain decreases the bandgap, and the Poisson effect would accelerate this process to some extent.

To have a systematic understanding of the bandgap evolution, the calculated bandgaps as a function of various loading strains are collected in Fig. 5. Generally speaking, similar to previous investigations,[57,58] the bandgap of silicon decreases remarkably as the loading strain increases and the magnitude of bandgap evolution shows strong anisotropy. Studies performed on small silicon nanowires also show the anisotropic bandgap depending on the growth orientations.[59]

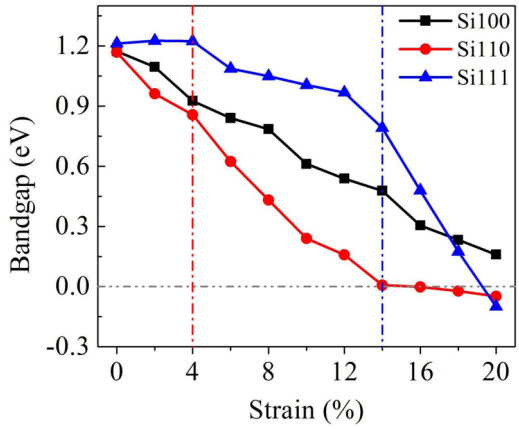

FIG. 5. Band structures of silicon under various loading strains along ⟨100⟩, ⟨110⟩, and ⟨111⟩ orientations. The vertical dashed lines denote the indirect to direct bandgap transition points.

The bandgap shows the most significant variation under the loading strain on the ⟨110⟩ orientation, and 4% loading strain is enough to achieve the indirect to direct bandgap transition. Moreover, as the loading strain on the ⟨110⟩ orientation reaches 14%, the bandgap will vanish leading to semiconductor to metal transition. The indirect to direct bandgap transition occurs with the strain on the ⟨111⟩ orientation as well and the transition point is at 14%. Similarly, the loading strain on silicon ⟨111⟩ will cause metallization at 20%. Initially, the bandgaps E_g under ⟨111⟩ strain change relatively slower than the other two direction strains, following the sequence $E_g^{\langle 111\rangle} > E_g^{\langle 100\rangle} > E_g^{\langle 110\rangle}$. However, the indirect bandgaps under ⟨111⟩ strain decrease dramatically after transition to direct bandgap. Therefore, we can conclude that tuning the electronic properties of silicon through applying strain on ⟨110⟩ orientations is easier than the other two orientations.

CONCLUSION

To summarize, the structural and electronic properties of silicon under various strains are comparatively investigated. We investigated the Poisson effect under elastic strain along the different orientations. The strain along the ⟨110⟩ orientation induces the largest cross section variation, while the strain along ⟨111⟩ shows the smallest. The band structures demonstrate an interesting correlation with the loading strain. Overall, the bandgaps gradually decrease as the loading strain increases on three directions, whereas the bandgap evolutions are different. Silicon keeps indirect bandgap with the loading strain along the ⟨100⟩ orientation. However, the strain along ⟨110⟩ and ⟨111⟩ achieves indirect to direct bandgap transition. The corresponding transition points are at 4% and 14% loading strains. More interestingly, the ultralarge strain would realize metallization in silicon under 14% strain along ⟨110⟩ and 20% along ⟨111⟩. Our calculations provide useful information for tuning the electronic and optical properties of silicon nanowire

through strain engineering experimentally. Silicon nanowires with different growth directions show electronically anisotropic response to external loading strain. We anticipate that the present work will stimulate further investigations on potential optical and optoelectronic applications of silicon nanowires via elastic strain engineering.

SUPPLEMENTARY MATERIAL

See supplementary material for the high symmetry k-point paths of the ⟨100⟩, ⟨110⟩, and ⟨111⟩ models and the six-fold energy surfaces diagram of the conduction band of bulk silicon.

ACKNOWLEDGMENTS

This research was supported by the Research Grants Council of the Hong Kong Special Administrative Region, China under the project CityU (No. 11216515). A.H. acknowledges the funding support from the City University of Hong Kong under Project No. 9610336. The authors declare no conflict of interest in this paper.

REFERENCES

[1]S. Hao, L. Cui, D. Jiang, X. Han, Y. Ren, J. Jiang, Y. Liu, Z. Liu, S. Mao, Y. Wang, Y. Li, X. Ren, X. Ding, S. Wang, C. Yu, X. Shi, M. Du, F. Yang, Y. Zheng, Z. Zhang, X. Li, D. E. Brown, and J. Li, Science **339**, 1191 (2013).
[2]F. Guinea, M. I. Katsnelson, and A. K. Geim, Nat. Phys. **6**, 30 (2009).
[3]A. H. Ghadimi, S. A. Fedorov, N. J. Engelsen, M. J. Bereyhi, R. Schilling, D. J. Wilson, and T. J. Kippenberg, Science **360**, 764 (2018).
[4]J. Li, Z. Shan, and E. Ma, MRS Bull. **39**, 108 (2014).
[5]A. Banerjee, D. Bernoulli, H. Zhang, M.-F. Yuen, J. Liu, J. Dong, F. Ding, J. Lu, M. Dao, W. Zhang, Y. Lu, and S. Suresh, Science **360**, 300 (2018).
[6]H. Zhang, J. Tersoff, S. Xu, H. Chen, Q. Zhang, K. Zhang, Y. Yang, C.-S. Lee, K.-N. Tu, J. Li, and Y. Lu, Sci. Adv. **2**, e1501382 (2016).
[7]N. Matsuhisa, M. Kaltenbrunner, T. Yokota, H. Jinno, K. Kuribara, T. Sekitani, and T. Someya, Nat. Commun. **6**, 7461 (2015).
[8]Y. Wu, A. R. Chew, G. A. Rojas, G. Sini, G. Haugstad, A. Belianinov, S. V. Kalinin, H. Li, C. Risko, J.-L. Brédas, A. Salleo, and C. D. Frisbie, Nat. Commun. **7**, 10270 (2016).
[9]S. E. Thompson, M. Armstrong, C. Auth, S. Cea, R. Chau, G. Glass, T. Hoffman, J. Klaus, M. Zhiyong, B. Mcintyre, A. Murthy, B. Obradovic, L. Shifren, S. Sivakumar, S. Tyagi, T. Ghani, K. Mistry, M. Bohr, and Y. El-Mansy, IEEE Electron Device Lett. **25**, 191 (2004).
[10]M. M. Roberts, L. J. Klein, D. E. Savage, K. A. Slinker, M. Friesen, G. Celler, M. A. Eriksson, and M. G. Lagally, Nat. Mater. **5**, 388 (2006).
[11]R. A. Minamisawa, M. J. Süess, R. Spolenak, J. Faist, C. David, J. Gobrecht, K. K. Bourdelle, and H. Sigg, Nat. Commun. **3**, 1096 (2012).
[12]Y. Cui, Z. Zhong, D. Wang, W. U. Wang, and C. M. Lieber, Nano Lett. **3**, 149 (2003).
[13]J. Juan-Colás, A. Parkin, K. E. Dunn, M. G. Scullion, T. F. Krauss, and S. D. Johnson, Nat. Commun. **7**, 12769 (2016).
[14]J. J. Ackert, D. J. Thomson, L. Shen, A. C. Peacock, P. E. Jessop, G. T. Reed, G. Z. Mashanovich, and A. P. Knights, Nat. Photonics **9**, 393 (2015).
[15]D.-M. Tang, C.-L. Ren, M.-S. Wang, X. Wei, N. Kawamoto, C. Liu, Y. Bando, M. Mitome, N. Fukata, and D. Golberg, Nano Lett. **12**, 1898 (2012).
[16]Y. Zhu, F. Xu, Q. Qin, W. Y. Fung, and W. Lu, Nano Lett. **9**, 3934 (2009).
[17]L. Tian, J. Li, J. Sun, E. Ma, and Z.-W. Shan, Sci. Rep. **3**, 2113 (2013).
[18]H. Zhang, K.-Y. Fung, Y. Zhuang, K. Cao, J. Song, A. Hu, and Y. Lu, Acta Mech. (published online, 2017).
[19]D. Roundy and M. L. Cohen, Phys. Rev. B **64**, 212103 (2001).
[20]S. M. M. Dubois, G. M. Rignanese, T. Pardoen, and J. C. Charlier, Phys. Rev. B **74**, 235203 (2006).
[21]Y. Umeno, A. Kushima, T. Kitamura, P. Gumbsch, and J. Li, Phys. Rev. B **72**, 165431 (2005).
[22]X. Luo, Z. Liu, B. Xu, D. Yu, Y. Tian, H.-T. Wang, and J. He, J. Phys. Chem. C **114**, 17851 (2010).
[23]J. Xue, Z. Jijun, and J. Xin, Nanotechnology **22**, 405705 (2011).
[24]J. Guo, B. Wen, R. Melnik, S. Yao, and T. Li, Diam. Relat. Mater. **20**, 551 (2011).
[25]X. Liu, L. Li, Q. Li, Y. Li, and F. Lu, Mater. Sci. Semicond. Process. **16**, 1369 (2013).
[26]I. J. T. Jensen, A. G. Ulyashin, and O. M. Løvvik, J. Appl. Phys. **119**, 015702 (2016).
[27]K.-H. Hong, J. Kim, S.-H. Lee, and J. K. Shin, Nano Lett. **8**, 1335 (2008).
[28]D. Yu, Y. Zhang, and F. Liu, Phys. Rev. B **78**, 245204 (2008).
[29]R. S. Jacobsen, K. N. Andersen, P. I. Borel, J. Fage-Pedersen, L. H. Frandsen, O. Hansen, M. Kristensen, A. V. Lavrinenko, G. Moulin, H. Ou, C. Peucheret, B. Zsigri, and A. Bjarklev, Nature **441**, 199 (2006).
[30]P. W. Leu, A. Svizhenko, and K. Cho, Phys. Rev. B **77**, 235305 (2008).
[31]R. Rurali and N. Lorente, Phys. Rev. Lett. **94**, 026805 (2005).
[32]M. Nolan, S. O'Callaghan, G. Fagas, J. C. Greer, and T. Frauenheim, Nano Lett. **7**, 34 (2007).
[33]M.-F. Ng, L. Y. Sim, H. Da, H. Jin, K. H. Lim, and S.-W. Yang, Theor. Chem. Acc. **127**, 689 (2010).
[34]Z. Keenan and C. Mei-Yin, J. Phys. Condens. Matter **25**, 145501 (2013).
[35]G. Kresse and J. Furthmüller, Comput. Mater. Sci. **6**, 15 (1996).
[36]G. Kresse and J. Furthmüller, Phys. Rev. B **54**, 11169 (1996).
[37]P. E. Blöchl, O. Jepsen, and O. K. Andersen, Phys. Rev. B **49**, 16223 (1994).
[38]G. Kresse and D. Joubert, Phys. Rev. B **59**, 1758 (1999).
[39]J. P. Perdew, K. Burke, and M. Ernzerhof, Phys. Rev. Lett. **77**, 3865 (1996).
[40]X. Wang, M. Dvorak, and Z. Wu, Phys. Rev. B **94**, 195429 (2016).
[41]Z.-h. Yang, H. Peng, J. Sun, and J. P. Perdew, Phys. Rev. B **93**, 205205 (2016).
[42]J. Heyd, G. E. Scuseria, and M. Ernzerhof, J. Chem. Phys. **118**, 8207 (2003).
[43]A. V. Krukau, O. A. Vydrov, A. F. Izmaylov, and G. E. Scuseria, J. Chem. Phys. **125**, 224106 (2006).
[44]J. Sun, B. Xiao, and A. Ruzsinszky, J. Chem. Phys. **137**, 051101 (2012).
[45]J. Sun, R. Haunschild, B. Xiao, I. W. Bulik, G. E. Scuseria, and J. P. Perdew, J. Chem. Phys. **138**, 044113 (2013).
[46]R. Rurali, A. Poissier, and N. Lorente, Phys. Rev. B **74**, 165324 (2006).
[47]M.-F. Ng, M. B. Sullivan, S. W. Tong, and P. Wu, Nano Lett. **11**, 4794 (2011).
[48]L. Lin, Z. Li, J. Feng, and Z. Zhang, Phys. Chem. Chem. Phys. **15**, 6063 (2013).
[49]S. Li, H. Zhang, J.-P. Chou, J. Wei, Y. Lu, and A. Hu, J. Phys. Chem. C **122**, 15780 (2018).
[50]J. Kioseoglou, T. Pavloudis, T. Kehagias, P. Komninou, T. Karakostas, C. D. Latham, M. J. Rayson, P. R. Briddon, and M. Eickhoff, J. Appl. Phys. **118**, 034301 (2015).
[51]J. J. Wortman and R. A. Evans, J. Appl. Phys. **36**, 153 (1965).
[52]H. J. McSkimin and P. Andreatch, J. Appl. Phys. **35**, 3312 (1964).
[53]W. Setyawan and S. Curtarolo, Comput. Mater. Sci. **49**, 299 (2010).
[54]M. V. Fischetti and S. E. Laux, J. Appl. Phys. **80**, 2234 (1996).
[55]P. S. Yadav, R. K. Yadav, S. Agrawal, and B. K. Agrawal, Prog. Cryst. Growth Charact. Mater. **52**, 10 (2006).
[56]J. L. Corkill and M. L. Cohen, Phys. Rev. B **47**, 10304 (1993).
[57]X. Zhao, C. M. Wei, L. Yang, and M. Y. Chou, Phys. Rev. Lett. **92**, 236805 (2004).
[58]P. W. Leu, B. Shan, and K. Cho, Phys. Rev. B **73**, 195320 (2006).
[59]R. Rurali, Rev. Mod. Phys. **82**, 427 (2010).